Front. Phys. China, 2007, 2(3): 279−288
DOI 10.1007/s11467-007-0044-l

REVIEW ARTICLE

GU Ben-yuan, ZHAO Li-ming

Second harmonic generations in aperiodic optical superlattices with finite width and in one-dimensional defective photonic crystals made of nonlinear optical materials

Abstract The characteristics of the second harmonic generations (SHGs) in homogeneous and inhomogeneous systems are investigated. We consider two kinds of structures: one is aperiodic optical superlattices (AOSs) with homogeneous linear susceptibility and the modulated second-order nonlinear susceptibility; the second is linear and nonlinear susceptibilities both the system with inhomogeneous. We derive a general solution of SHG for the AOS with finite lateral width and of SHG in considering the depletion of the pump light power. We carry out the design of AOSs by using simulation annealing (SA) algorithm and show that the constructed AOSs can implement multiple wavelength SHGs with identical effective nonlinear coefficient at the preassigned wavelengths of incident light. We observe great enhancement of SHGs in the one-dimensional photonic crystals (PCs) with defects consisting of multiple photonic quantum wells made of nonlinear material when the frequency of fundamental wave aims at one of the defect states. We also propose an effective design approach of aperiodically stacked layers of nonlinear material and air in terms of the SA method. The constructed structure can achieve multiple-wavelength SHGs at the preassigned wavelengths.

Keywords second-harmonic-generation, aperiodic-optical-superlattices, finite-width, defective-photonic-crystal

PACS numbers 42.65.Ky, 42.79.Nv, 77.80.Dj, 78.66.-w

1 Introduction

Finding a laser source at new wavelengths is an Important issue, which can be achieved by nonlinear optical processes. In the conventional method, phase-matching (PM) condition is required for gaining high conversion efficiency [1, 2], however, the PM condition brings a big restriction to the choice of natural birefringent material. Another scheme is the so-called quasi-phase matching (QPM) [3, 4], which can significantly diversify the class of nonlinear optical materials [5−13]. Some groups of researchers have successfully achieved the design of aperiodic optical superlattices (AOSs) for multiple wavelength second harmonic generations (SHGs) [14, 15]. The design result has been confirmed by experiment [16].

Photonic crystals (PCs) with periodic modulated dielectric function have attracted considerable interest because of many novel effects in the aspects of fundamental physics and potential applications. Previous studies on SHGs in PCs were mainly focused on the characteristics of the second harmonic wave (SHW) when the frequency of the fundamental wave (FW) approaches the band edge of PCs. The density of the electromagnetic (EM) field modes becomes much larger and the fields are highly localized, thus, the conversion efficiency should be enhanced significantly [17−19]. If a defect structure made of nonlinear material is introduced into the PCs, some defect states within the photonic band gap (PBG) are created and give rise to strong localized fields. In this system, it is expected that the conversion efficiency might be increased considerably [20].

The propagation of nonlinear waves in nonlinear crystals is governed by the coupled-wave equations, which are based on Maxwell's equations. Several simplifying approximations are often adopted, for instance, the infinite plane wave approximation (IPWA), small signal approximation (SSA), and slowly varying amplitude approximation (SVAA), etc. However, in practical applications, the optical superlattices always

GU Ben-yuan (✉), ZHAO Li-ming
Institute of Physics, Chinese Academy of Sciences, P. O. Box 603, Beijing 100080, China
E-mail: guby@aphy.iphy.ac.cn

Received March 10, 2007

possess finite lateral width. Under high pump power, it is desirable to expand the beam size in a large extension to avoid optical damage of nonlinear crystals. Therefore, the effects of the finite lateral width of the AOSs and the mode-mode coupling on the SHGs could be important. For the SSA, the depletion of FW power in the SHGs is neglected; this approximation should lead to a big restriction to the signal intensity of SHG because it requires a low pumping level of the FW. In an inhomogeneous system, the reflection of SHW at interfaces is so strong that the SVAA may bring inaccurate results [21].

In this review article, we report the design of AOSs with finite width [22] for implementing multiple-wavelength SHGs with identical effective nonlinear coefficients, by using simulated annealing (SA) algorithm [23, 24]. The characteristics of SHGs in samples are studied under the large, intermediate, and small signal levels of the FW [25]. We present a general solution to the SHG in one-dimensional (1D) inhomogeneous systems and apply it to investigate the SHGs in the samples composed of multiple photonic quantum-wells (PQWs) made of ferroelectric nonlinear material, i.e., defective structures [26]. It is found that the conversion efficiency of SHG can be greatly enhanced when the FW frequency is aimed at one of the defect states. Both "forward" and "backward" SHGs can be controlled by adjusting the polarization directions of ferroelectric domains. We also propose an efficient design approach of aperiodically stacked-layer structures of nonlinear material and air, sandwiched by two truncated PCs, in terms of the SA method. The constructed structure can achieve multiple wavelength SHGs simultaneously at the preassigned wavelengths with high conversion efficiency [27].

2 Model structures and fundamental formulas

We first revisit the SHG formulas in AOSs made of alternating laminar domains of ferroelectric crystals, for instance, $LiNbO_3$ (LN) or $LiTaO_3$ (LT) crystals, under IPWA, SSA, and SVAA. Assume that a laser beam with $\omega_1 = \omega$ is normally launched upon an AOS and through the nonlinear optical process, the SHG is generated. In order to use the largest nonlinear coefficient of these materials, d_{33}, let the interfaces of domains be parallel to the yz plane; the propagation and the polarization directions of the incident light are along the x and z axes, respectively. The modulation of the nonlinear optical coefficient d_{33} in the AOS is described by $\chi(x) = \chi_j$ in the jth unit block for $x_{j-1} \leqslant x \leqslant x_j$, and χ_j takes only a binary value, d_{33} or $-d_{33}$, corresponding to the positive or negative polarization. We denote $x_0 = 0$ and $x_N = L = N\Delta x$, where L is the length of the AOS sample; N is the number of the unit blocks in sample; Δx denotes the thickness of each individual unit block. In the so-called small-signal approximation, in which the depletion loss of fundamental wave power can be negligible, the electric field $E_{1\omega}(x)$ [$E_{2,\omega}(x)$] of the FW (SHW) satisfies the following wave equations:

$$\left(\frac{\mathrm{d}^2}{\mathrm{d}x^2} + k_{1\omega}^2\right) E_{1\omega}(x) = 0 \tag{2.1}$$

$$\left(\frac{\mathrm{d}^2}{\mathrm{d}x^2} + k_{2\omega}^2\right) E_{2\omega}(x) = -k_{20}^2 \chi(x) E_{1\omega}^2(x) \tag{2.2}$$

where $k_{10} = \omega/c$, ($k_{20} = 2\omega/c$), and $k_{1\omega} = n_{1\omega}k_{10}$, ($k_{2\omega} = n_{2\omega}k_{20}$), c is the light speed in vacuum, $n_{1\omega} = n(\omega)$, [$n_{2\omega} = n(2\omega)$] is the refractive index of the material at the FW (SHW) frequency. In the SVAA, the conversion efficiency η_{SHG} from FW with wavelength λ and intensity $I_{1\omega}$ to SHW reads [15, 16]

$$\eta_{\mathrm{SHG}} = C_s Q^2(\lambda) \xi_{eff}^{(s)}(\lambda) \tag{2.3}$$

with

$$C_s = \frac{8\pi^2 |d_{33}|^2 I_{1\omega} L^2}{c\epsilon_0} \tag{2.4}$$

and

$$Q(\lambda) = \frac{1}{\lambda\sqrt{n_{2\omega}} n_{1\omega}} \tag{2.5}$$

$$\xi_{\mathrm{eff}}^{(s)}(\lambda) = |\frac{1}{L}\int_0^L \mathrm{d}x \mathrm{e}^{\mathrm{i}[2\pi x/l_c^{(s)}(\lambda)]} \widetilde{d}(x)|^2 \tag{2.6}$$

and $l_c^{(s)}(\lambda) = 2\pi/(k_{2\omega} - 2k_{1\omega})$.

The optimal configuration of $\widetilde{d}(x)$ in the sample is determined by the SA algorithm.

2.1 SHG and multiple mode effects in AOS with finite lateral width

We consider the SHGs from an AOS with a finite lateral width W. In a direct non-depleted pump wave approximation, the electric field $E_{1\omega}(x, y)$ [$E_{2\omega}(x, y)$] of the FW (SHW) in the quasi-1D AOS satisfies the following homogeneous or inhomogeneous wave equation:

$$\left(\frac{\mathrm{d}^2}{\mathrm{d}x^2} + \frac{\mathrm{d}^2}{\mathrm{d}y^2} + k_{1\omega}^2\right) E_{1\omega}(x, y) = 0 \tag{2.1.1}$$

$$\left(\frac{\mathrm{d}^2}{\mathrm{d}x^2} + \frac{\mathrm{d}^2}{\mathrm{d}y^2} + k_{2\omega}^2\right) E_{2\omega}(x, y) = -k_{20}^2 \chi(x) E_{1\omega}^2(x, y) \tag{2.1.2}$$

In the air region, the fields E_{1g} (E_{2g}) of FW (SHW) satisfies the following equations:

$$\left(\frac{\mathrm{d}^2}{\mathrm{d}x^2}+\frac{\mathrm{d}^2}{\mathrm{d}y^2}+k_{10}^2\right)E_{1g}(x,y)=0 \tag{2.1.3}$$

$$\left(\frac{\mathrm{d}^2}{\mathrm{d}x^2}+\frac{\mathrm{d}^2}{\mathrm{d}y^2}+k_{20}^2\right)E_{2g}(x,y)=0 \tag{2.1.4}$$

The boundary conditions at interfaces are

$$\begin{aligned}
&E_{1\omega}\left(x,y=\pm\frac{W}{2}\right)=E_{1g}\left(x,y=\pm\frac{W}{2}\right)\\
&\frac{\partial E_{1\omega}}{\partial y}\left(x,y=\pm\frac{W}{2}\right)=\frac{\partial E_{1g}}{\partial y}\left(x,y=\pm\frac{W}{2}\right)\\
&E_{2\omega}\left(x,y=\pm\frac{W}{2}\right)=E_{2g}\left(x,y=\pm\frac{W}{2}\right)\\
&\frac{\partial E_{2\omega}}{\partial y}\left(x,y=\pm\frac{W}{2}\right)=\frac{\partial E_{2g}}{\partial y}(x,y=\pm\tfrac{W}{2})
\end{aligned} \tag{2.1.5}$$

For the field of FW, there exist two styles of modes. One is the guided mode, which is confined in the interior of the sample, and the other is the radiation mode. We focus on the contribution of the guided mode to the SHG because the energy of the radiation mode in the AOS is quite weak. To solve Eq. (2.1.1), we expand $E_{1\omega}(x,y)$ in terms of transverse eigen modes

$$\phi_{1n}(y)=\rho_{1n}\cos\left[\kappa_{1n}\left(y+\frac{W}{2}\right)+\arctan\frac{\beta_{1n}}{\kappa_{1n}}\right]$$

as

$$E_{1\omega}(x,y)=\Sigma_n a_n \mathrm{e}^{\mathrm{i}p_{1n}x}\phi_{1n}(y) \tag{2.1.6}$$

where

$$\rho_{1n}=\sqrt{\frac{2}{W+\frac{\sin\left(2\arctan\frac{\beta_{1n}}{\kappa_1}\right)}{\kappa_{1n}}}+\frac{2\cos^2\left(\arctan\frac{\beta_{1n}}{\kappa_{1n}}\right)}{\beta_{1n}}}$$

$p_{1n}^2=k_{1\omega}^2-\kappa_{1n}^2$, $\beta_{1n}^2=p_{1n}^2-k_{10}^2$, κ_{1n} and β_{1n} satisfy the following equation: $\kappa_{1n}=\frac{1}{W}\left(n\pi-2\arctan\frac{\beta_{1n}}{\kappa_{1n}}\right)$, a_n is the expansion coefficient. The solution of inhomogeneous equation Eq. (2.1.2) can then be expressed in general as

$$E_{2\omega}(x,y)=\Sigma_n b_n(x)\mathrm{e}^{\mathrm{i}p_{2n}x}\phi_{2n}(y) \tag{2.1.7}$$

where p_{2n}, ϕ_{2n}, κ_{2n} have the similar expressions respectively as $p_{1n}(y)$, $\phi_{1n}(y)$, κ_{1n}.

In the SVAA of the SHW field, through the standard manipulations, the conversion efficiency of SHG can also be expressed as Eq. (2.3), but the $\xi_{\mathrm{eff}}(\lambda)$ should be modified by

$$\xi_{\mathrm{eff}}^{(s)}(\lambda)=\sum_{n,l_1,l_2,m_1,m_2}\frac{k_{2\omega}^2}{p_{2n}^2}\cdot A_{l_1}A_{l_2}^*A_{m_1}A_{m_2}^*$$

$$G_{l_1m_1n}G_{l_2m_2n}F_{l_1m_1n}(L)F_{l_2m_2n}^*(L) \tag{2.1.8}$$

where

$$F_{lms}(x)=\frac{1}{L}\int_0^x \mathrm{d}\zeta\widetilde{\mathrm{d}}(\zeta)\mathrm{e}^{\mathrm{i}(p_{1l}+p_{1m}-p_{2s})\zeta}$$

and G_{lms} is evaluated by

$$\begin{aligned}
G_{lms}&=\sqrt{W}\int_{-W/2}^{W/2}\mathrm{d}y\phi_s(y)\phi_m(y)\phi_l(y)\\
&=\frac{1}{4}W^{3/2}\rho_{1m}\rho_{1l}\rho_{2s}\Big\{\mathrm{sinc}[(\kappa_{1l}+\kappa_{1m}+\kappa_{2s})W/2]\\
&\quad+\mathrm{sinc}[(\kappa_{1l}+\kappa_{1m}-\kappa_{2s})W/2]\\
&\quad+\mathrm{sinc}[(\kappa_{1l}-\kappa_{1m}+\kappa_{2s})W/2]\\
&\quad+\mathrm{sinc}[(\kappa_{1l}+\kappa_{1m}-\kappa_{2s})W/2]\Big\}
\end{aligned}$$

where $\sin\mathrm{c}(y)=\sin(y)/y$. $A_n=a_n/\sqrt{\sum_m|a_m|^2}$ and $|A|_n^2$ represents the weight ratio of the nth-mode intensity to FW intensity. We assume that a beam of light wave with a Gaussian profile of $E=\mathrm{e}^{-\frac{y^2}{\sigma^2}}\exp(\mathrm{i}kx)$ impinges normally upon the surface of the sample, then the corresponding mode amplitude of the FW field is given by $A_n=\rho_{1n}\int_{-W/2}^{W/2}\mathrm{d}y\mathrm{e}^{-\frac{y^2}{\sigma^2}}\cos(\kappa_{1n}y)\Big/\int_{-W/2}^{W/2}\mathrm{d}y\mathrm{e}^{-\frac{2y^2}{\sigma^2}}$. A_n has non-zero value only when $n=0,2,4,6,\cdots,=$ even. For convenience, we denote the maximum mode index as N_c (an even number), i.e., taking $l_1,l_2,m_1,m_2=0,2,4,6,\cdots,N_c$ into account in the summation in Eq. (2.1.8), the contribution of the higher index mode can be negligible.

2.2 SHG conversion efficiency in considering the depletion of pumping light power

In the SVAA, the equations governing the propagation of the FW and the SHW in the 1D AOS read

$$\frac{\mathrm{d}E_{1\omega}(x)}{\mathrm{d}x}=\frac{\mathrm{i}\omega_{1\omega}^2\chi(x)}{k_{1\omega}c^2}E_{2\omega}(x)E_{1\omega}^*(x)\mathrm{e}^{\mathrm{i}\Delta kx} \tag{2.2.1}$$

$$\frac{\mathrm{d}E_{2\omega}(x)}{\mathrm{d}x}=\frac{\mathrm{i}\omega_{2\omega}^2\chi(x)}{2k_{2\omega}c^2}E_{1\omega}^2(x)\mathrm{e}^{-\mathrm{i}\Delta kx} \tag{2.2.2}$$

where $\Delta k=k_{2\omega}-2k_{1\omega}$. In the AOS sample, we have $\chi(x)=|d_{33}|\widetilde{d}(x)$.

We assume the formal solution to Eqs. (2.2.1) and (2.2.2) as

$$E_{\alpha\omega}(x)=\rho_{\alpha\omega}(x)\mathrm{e}^{\mathrm{i}\phi_{\alpha\omega}(x)},\quad \alpha=1,2$$

we define

$$\theta(x)=\Delta kx-\phi_2(x)-\phi_1(x)$$

Total intensity (the power of per unit area) of two EM fields is

$$I=I_1+I_2=\text{constant}$$

with

$$I_{\alpha\omega} = 0.5\epsilon_0 c^2 k_{\alpha\omega}\rho_{\alpha\omega}^2/\omega_\alpha, \quad \alpha = 1, 2$$

where ϵ_0 is the permittivity of vacuum. We introduce the variable replacements

$$u_{\alpha\omega}(x) = \sqrt{I_{\alpha\omega}/I} = \left(\frac{\epsilon_0 c^2 k_{\alpha\omega}}{2\omega_\alpha I}\right)^{1/2} \rho_{\alpha\omega}(x), \quad \alpha = 1, 2$$

where $u_{\alpha\omega}^2(x)$ denotes the normalized intensity. It is clearly seen that $u_{1\omega}^2(x) + u_{2\omega}^2(x) = 1$. Therefore, the conversion efficiency is given by

$$\eta = u_{2\omega}^2(L) \tag{2.2.3}$$

When introducing

$$\zeta(x) = K(x)x \text{ and } K(x) = \left(\frac{8\pi^2 I}{\epsilon_0 c\lambda^2 n_{1\omega}^2 n_{2\omega}}\right)^{1/2} \chi(x)$$

through the standard manipulations, the solution of $\cos\theta$ in the lth domain of AOS reads

$$\cos\theta^{(l)} = -\left(\frac{\Delta k}{2K_l}\right)\frac{u_{2\omega}^{(l)2} + \Gamma_l}{u_{1\omega}^{(l)2} u_{2\omega}^{(l)}} \tag{2.2.4}$$

where $u_2^{(l)}$ ($u_1^{(l)}$, K_l) stands for the value of $u_{2\omega}(x)$ ($u_{1\omega}(x)$, $K(x)$) in the lth domain. The initial condition requires $\Gamma_1 = 0$ because the intensity of SHW at the entrance of the sample should be zero. Here, we set $u_{2\omega}(x_q)$ to the value of $u_{2\omega}^{(q)}$ at the exit of the qth domain. The variations of θ along the x-axis should be continuous, therefore, from Eq. (2.2.4) we can obtain

$$\Gamma_{l+1} = \begin{cases} \Gamma_l, & \text{when the consecutive domains} \\ & \text{have identical polarization} \\ -2u_{2\omega}^2(x_l) - \Gamma_l, & \text{otherwise} \end{cases} \tag{2.2.5}$$

Through the standard manipulation, we have

$$u_{2\omega}^{'}(x_l) = \mathrm{sn}[y, \beta] \tag{2.2.6}$$

where

$$y = \pm(u_c^2 - u_a^2)^{1/2}\Delta\zeta + A_0 \tag{2.2.7}$$

where $\Delta\zeta = K(x_l)N\Delta x$, and "$\pm$" is determined by the sign of $\sin\theta$; $\beta = (u_b^2 - u_a^2)/(u_c^2 - u_a^2)$, and $u_a,\ u_b,\ u_c$ ($u_a < u_b < u_c$) denote the three roots of the following equation:

$$u_{2\omega}^2(1 - u_{2\omega}^2)^2 - \frac{\Delta k^2}{4K^2}(u_{2\omega}^2 + \Gamma)^2 = 0$$

In Eqs. (2.2.6) and (2.2.7), we denote

$$u_{2\omega}^{'2} = \frac{u_{2\omega}^2 - u_a^2}{u_b^2 - u_a^2} \tag{2.2.8}$$

and

$$A_0 = \int_0^{u_{2\omega}^{'}(x_{l-1})} \frac{\mathrm{d}u_{2\omega}^{'}}{\sqrt{(1-u_{2\omega}^{'2})[1-(u_b^2-u_a^2)(u_c^2-u_a^2)^{-1}u_{2\omega}^{'2}]}} \tag{2.2.9}$$

the function of $\mathrm{sn}(z, \kappa)$ is defined by

$$z = \int_0^w \frac{\mathrm{d}t}{[(1-t^2)(1-\kappa^2 t^2)]^{1/2}}, \quad \omega = \mathrm{sn}(z, \kappa)$$

It is worth emphasizing that all the equations appearing in the above expressions belong to the lth domain; sometimes we omit this index for simplicity.

2.3 SHGs in 1D inhomogenous systems

The typical samples considered are composed of alternatingly stacked dielectric-dielectric with different dielectric indices or dielectric-air layers. We assume that the interface of layers is laid on the yz plane. The incident light is normally launched upon the surface of the sample. In a direct non-depleted pump wave approximation, for the lth layer, the FW (SHW) electric field $E_{1\omega}^{(l)}(x)$ ($E_{2\omega}^{(l)}(x)$) satisfies the following equations:

$$\left(\frac{\mathrm{d}^2}{\mathrm{d}x^2} + k_{1\omega}^{(l)2}\right)E_{1\omega}^{(l)}(x) = 0 \tag{2.3.1}$$

$$\left(\frac{\mathrm{d}^2}{\mathrm{d}x^2} + k_{2\omega}^{(l)2}\right)E_{2\omega}^{(l)}(x) = -k_{20}^2\chi_l E_{1\omega}^{(l)2}(x) \tag{2.3.2}$$

where $k_{1\omega}^{(l)} = n_{1\omega}^{(l)}k_{10}$, $k_{2\omega}^{(l)} = n_{2\omega}^{(l)}k_{20}$, $k_{10} = \omega/c$, and $k_{20} = 2\omega/c$. c is the light velocity in vacuum; $n_{1\omega}^{(l)}$ ($n_{2\omega}^{(l)}$) is the refractive index of the lth layer material at the FW (SHW) frequency; χ_l is the nonlinear optical coefficient of the lth layer material.

The FW electrical field in the lth layer of the sample can be expressed as

$$E_{1\omega}^{(l)}(x) = A_{1\omega}^{(l)}\mathrm{e}^{\mathrm{i}k_{1\omega}^{(l)}(x-x_{l-1})} + B_{1\omega}^{(l)}\mathrm{e}^{-\mathrm{i}k_{1\omega}^{(l)}(x-x_{l-1})} \tag{2.3.3}$$

where x_1 sets 0, $x_l = x_{l-1} + d_l$ ($l = 2, 3, \cdots$), d_l is the thickness of the lth layer. $A_{1\omega}^{(l)}$ and $B_{1\omega}^{(l)}$ respectively represent the amplitudes of the "forward" and "backward" FW waves at interface. By using the continuity of the fields at interfaces and the initial condition of $A_{1\omega}^{(1)} = 1$ and $B_{1\omega}^{(N)} = 0$, the amplitudes $A_{1\omega}^{(l)}$ and $B_{1\omega}^{(l)}$ of every layer can be completely determined. Noting that N denotes the total number of layers in the sample.

We now calculate the SHW electric field. In the lth layer, it can be expressed as a form of

$$E_{2\omega}^{(l)}(x) = A_{2\omega}^{(l)} \mathrm{e}^{\mathrm{i}k_{2\omega}^{(l)}(x-x_{l-1})} + B_{2\omega}^{(l)} \mathrm{e}^{-\mathrm{i}k_{2\omega}^{(l)}(x-x_{l-1})} + C_l \left[A_{1\omega}^{(l)2} \mathrm{e}^{\mathrm{i}2k_{1\omega}^{(l)}(x-x_{l-1})} + B_{1\omega}^{(l)2} \mathrm{e}^{-\mathrm{i}2k_{1\omega}^{(l)}(x-x_{l-1})} \right] - \frac{2k_{20}^2 \chi l}{k_{2\omega}^{(l)2}} A_{1\omega}^{(l)} B_{1\omega}^{(l)} \quad (2.3.4)$$

where $A_{2\omega}^{(l)}$ and $B_{2\omega}^{(l)}$ represent the amplitudes of the "forward" and "backward" SHWs, respectively. Substituting Eqs. (2.3.3) and (2.3.4) into Eq. (2.3.2), we obtain

$$C_l = \frac{-k_{20}^2 \chi l}{k_{2\omega}^{(l)2} - 4k_{1\omega}^{(l)2}} \quad (2.3.5)$$

Considering the continuity of the electric and magnetic fields at interface, and the initial condition $A_{2\omega}^{(1)} = 0$ and $B_{2\omega}^{(N)} = 0$, thus, $A_{2\omega}^{(l)}$ and $B_{2\omega}^{(l)}$ for each layer can be determined. The conversion efficiencies of the "forward" and "backward" waves are evaluated respectively by

$$\eta_{\mathrm{forth}} = \frac{n_{2\omega}^{(N)} |A_{2\omega}^{(N)}(x_{N-1})|^2}{n_{1\omega}^{(1)} |A_{1\omega}^{(1)}|^2}, \quad \eta_{\mathrm{back}} = \frac{|B_{2\omega}^{(1)}(x_1)|^2}{|A_{1\omega}^{(1)}|^2} \quad (2.3.6)$$

3 Results and analysis

3.1 SHGs in AOS with finite width

We now carry out a special design of the AOS made of $LiTaO_3$ (LT) crystal that achieves multiple wavelength SHGs with identical effective nonlinear coefficient $\xi_{\mathrm{eff}}^{(s)}(\lambda) = \xi^{(0)}$. First, we have to carefully choose an appropriate thickness Δx of the unit block. Δx is mainly decided by the maximum value of the function $\mathrm{sinc}[(p_{1l} + p_{1m} - p_{2n})\Delta x/2]$. This factor strongly depends on wavelength. As is well known, $\mathrm{sinc}(x) \sim 1$, when x is small enough, thus, this wavelength dependence can be negligible. Therefore, we choose $\Delta x = 3$ μm for matching with the state-of-the-art of microfabrication. The objective function used in the SA method is chosen as

$$D = \Sigma_\alpha [|\xi^{(0)} - \xi_{\mathrm{eff}}^{(s)}(\lambda_\alpha)|] + \gamma [\max\{\xi_{\mathrm{eff}}^{(s)}(\lambda_\alpha)\} - \min\{\xi_{\mathrm{eff}}^{(s)}(\lambda_\alpha)\}]$$

where the symbol $\max\{\cdots\}(\min\{\cdots\})$ manifests taking their maximum (minimum) value among all the quantities including into $\{\cdots\}$. γ is an adjustable parameter, taking a value of 0.3−3.0. λ_α is set to the following values: 0.9720, 1.0820,1.2830,1.3940, and 1.5687 μm. The refractive indices of LT crystal at the FW and SHW frequencies are calculated at $T = 25$ °C according to the Sellmeier formula given in Ref. [8].

We calculate the effective nonlinear coefficient for the incident FW beam with a Gaussian profile of $E = \mathrm{e}^{-\frac{y^2}{\sigma^2}} \mathrm{e}^{\mathrm{i}kx}$ and in the case of multiple modes. We adopt the parameters in the calculations as: The total length of sample $L = 3.0$ mm, the number of blocks $N = 10^3$, the width of superlattice $W = 1.0$ mm. Figure 1 displays the calculated reduced effective nonlinear coefficient in the case of $N_{\mathrm{c}} = 10$ as a function of wavelength. It exhibits almost identical-height peaks at the preassigned wavelengths after scanning a wide range of wavelengths from 0.85 μm to 1.65 μm with the resolution of 0.5 Å. It is also seen that there is one unexpected peak of $\lambda = 0.980\ 95$ μm appearing near the preset wavelength of $\lambda = 0.972\ 00$ μm.

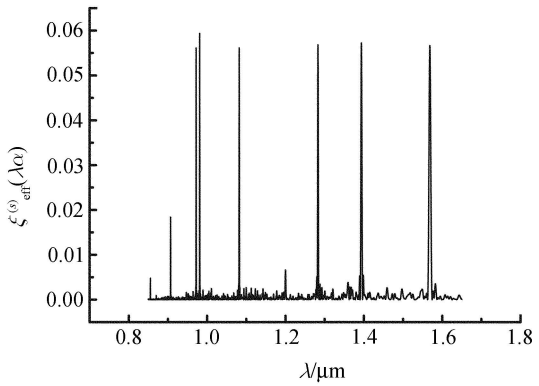

Fig. 1 Variations of $\xi_{\mathrm{eff}}^{(s)}(\lambda)$ with wavelength in the AOS made of $LiTaO_3$ (LT) crystal with a finite width W for implementing multiple wavelength SHGs with identical effective nonlinear coefficient. The incident FW beam has a Gaussian profile and we consider the case of multiple modes. The number of the modes is $N_{\mathrm{c}} = 10$.

In order to further reveal the characteristics of SHG in the constructed AOS, we demonstrate the variations of $\xi_{\mathrm{eff}}^{(s)}(\lambda)$ with the optical wave propagating distance x from the surface of the sample, as shown in Fig.2, for five main peaks of Fig.1. It is apparent that all curves exhibit the increasing behavior and with nearly identical rising slope. It hints that the orientation of domains is quite favorable to the SHG processes because the contribution of successive blocks to $\xi_{\mathrm{eff}}^{(s)}(\lambda)$ takes constructive accumulation.

The dependence of the effective nonlinear coefficient at the preassigned wavelength of the FW on the number of modes, N_{c}, is illustrated in Fig. 3 for different widths W of sample, $W = 0.5, 1.0, 1.5$, and 2.5 mm. The other parameters are as follows: $\Delta x = 3$ μm; $L = 3.0$ mm; $N = 10^3$; and $\sigma = 1.0$ mm. $\left\langle \xi_{\mathrm{eff}}^{(s)} \right\rangle$ abruptly decreases at the beginning and then tends to a constant with the increase of W. These results can be well interpreted: For a Gaussian profile beam, the light

energy is almost focused on a range of σ size. When the width W of the sample is smaller than $\sigma = 1.0$ mm, for example, $W = 0.5$ mm, the average intensity of the incident FW beam is relatively large at the entry of the sample, thus, the corresponding plateau value of the $\left\langle \xi_{\rm eff}^{(s)} \right\rangle$ should be big. However, when increasing the width of the sample, the average intensity of the incident FW beam is accordingly decreased, thus, the plateau value of the $\left\langle \xi_{\rm eff}^{(s)} \right\rangle$ is reduced. However, when $W > \sigma$, the change of the average intensity of the incident FW beam with W is small because the majority of the energy of the incident FW beam is only restricted to a range of σ, as a result, the variations of the plateau value of $\left\langle \xi_{\rm eff}^{(s)} \right\rangle$ with W now become quite weak, as seen in the curves corresponding to $W = 1.5$ and 2.5 mm in Fig. 3.

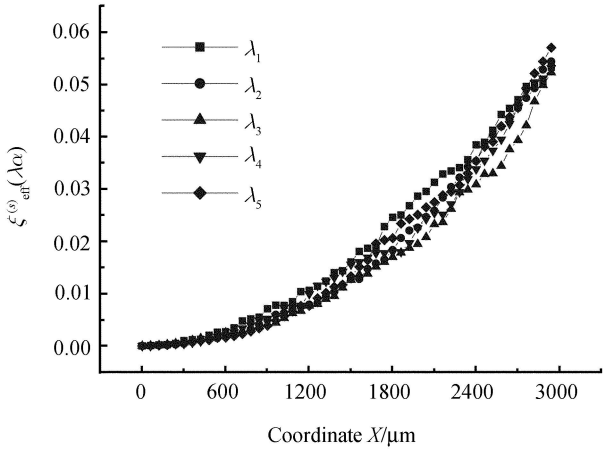

Fig. 2 Variations of $\xi_{\rm eff}^{(s)}(\lambda)$ with the optical wave propagating distance x from the surface of sample (given in Fig. 1) for five main peaks in Fig. 1.

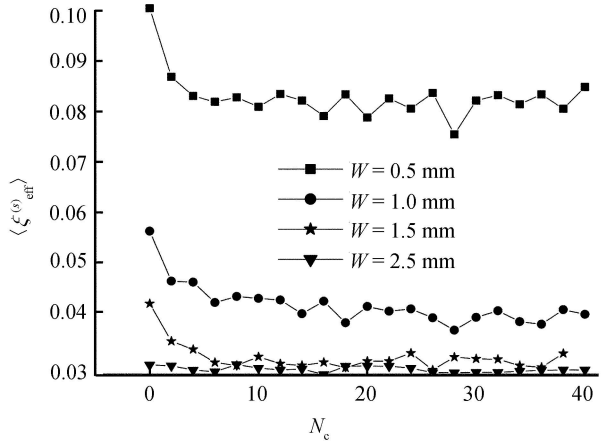

Fig.3 Dependence of the effective nonlinear coefficient at the preassigned wavelengths of the FW on the number of modes, $N_{\rm c}$, for different widths W of sample as the same in Fig.1: $W = 0.5, 1.0, 1.5,$ and 2.5 mm.

3.2 SHGs in considering the depletion of pumping light power

We carry out a specific model design of the AOS made of $LiNbO_3$ (LN) crystal by using the SA method for achieving multiple wavelength SHG with identical conversion efficiency under the consideration of the depletion of pump light power. The objective function used in the SA method is given by

$$D = \Sigma_\alpha[|\eta^{(0)} - \eta(\lambda_\alpha)|] + \gamma[\max\{\eta(\lambda_\alpha)\} - \min\{\eta(\lambda_\alpha)\}] \tag{3.2}$$

λ_α is the preassigned wavelength. $\eta^{(0)}$ is a preset constant. The optimization construction of the AOS for the SHG is ascribed to a search for the minimum of the objective function with respect to the thickness of every domain in the sample.

We calculate the SHG conversion efficiency of the designed AOS sample for the pre-assigned FW wavelengths: $\lambda_\alpha = 0.9720, 1.0820, 1.2830, 1.3940,$ and 1.5687 μm. The refractive indices of LN crystal at the FW and SHW frequencies are evaluated at $T = 25°$C according to the Sellmeier formula given in Ref. [8]. The total thickness of the sample is $L = 4.5$ mm, the number of domains $N = 1.5 \times 10^3$, the intensity of the incident light wave sets $I = 30.0(9.2, 1.8) \times 10^{11}$W/m^2 for the large (intermediate, small) signal level. $d_{33} = 47.0$ pm/V is referred to Ref. [28].

The wavelength–dependence of η is shown in Figure 4 for the above-mentioned three pump levels of FW. All exhibit almost identical-height peaks at the pre-assigned wavelengths after scanning a wide range of wavelengths from 0.85 to 1.65 μm with a step of 0.5 Å. However, there exists a remarkable difference: In the large signal regime, the η-λ plot contains many extra stray peaks (out-off the preassigned wavelengths), for instance, marked by λ_{e1}, λ_{e2}, λ_{e3}. There are a lot of small stray peaks over the range of $[0.85, 1.65]$ μm; meanwhile, the heavy background noise occurs in this plot, as shown in Fig. 4(a). The conversion efficiency peaks approach 1. In the regime of the intermediate signal, the main peak value of η is reduced to 0.72. The extra strong stray peak, λ_{e2}, still survives; at the same time, the background noise is substantially lowered, as shown in Fig.4(b). In the regime of the small signal, the main peak value of η is reduced to 0.31; the strong stray peaks now disappear; the strength of the background noise is remarkably suppressed to a much lower level, as seen in Fig. 4(c).

In order to further explore the characteristics of the SHG from the constructed AOS, the variations of the normalized intensities of SHW and FW with the optical wave propagating distance from the surface of the sample are depicted in Fig. 5 for the five preset wavelengths in three different pumping FW

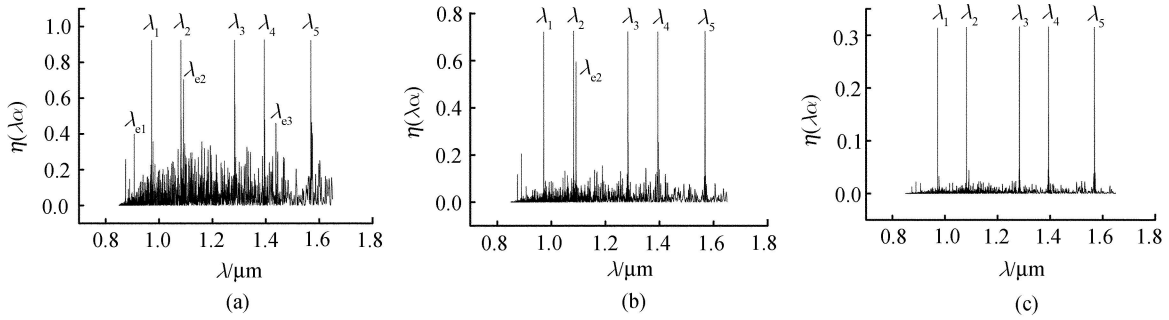

Fig. 4 Variations of the SHG conversion efficiency with the wavelength of the incident plane light waves in the AOS for achieving multiple wavelength SHGs with identical nonlinear coefficient under the consideration of the depletion of pump light power : **(a)**, **(b)**, and **(c)** correspond to the large (I=30.0×10^{11} W/m^2) intermediate (I=9.2×10^{11}W/m^2), and small (I=1.8×10^{11}W/m^2) pump signal levels of the FW, respectively. The AOS is made of $LiNbO_3$ (LN) crystal designed by the SA method.

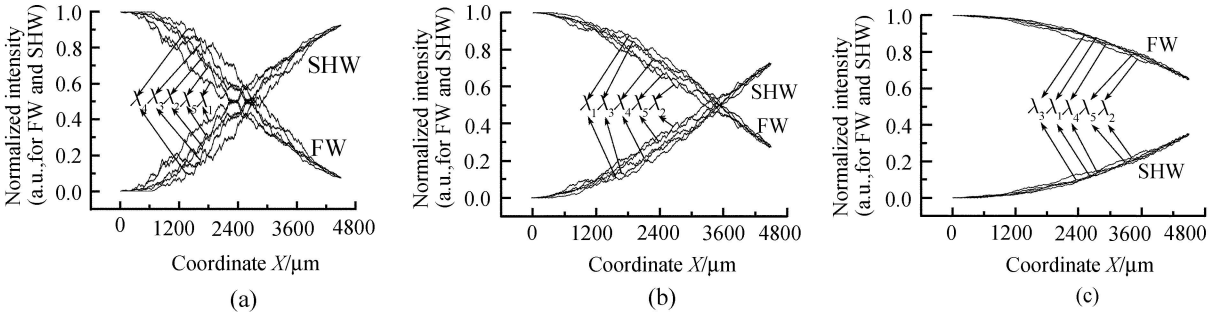

Fig. 5 Variations of the normalized intensities of SHW and FW with the optical wave propagating distance from the surface of sample, as the same as in Fig. 3, for the five preset wavelengths in three different pumping FW levels: **(a)**, **(b)**, and **(c)** correspond to the large, intermediate, and small pump levels of FW, respectively.

levels. It is evident that all curves for SHW (FW) exhibit nearly monotonically increasing (decreasing) behavior with a nearly identical slope. This implies that the contribution of each individual unit block domain takes a constructive addition. It confirms that the arrangement of domains is favorable to the SHG processes. The saturation effect of SHG is also observed in Fig. 5(a) at a large signal level.

3.3 Great enhancement of SHGs in defective 1D PCs

We now turn to explore the feature of SHGs in the sample, which is composed of alternatingly stacked dielectric-air-nonlinear material layers with finite number and surrounded by air. For convenience, we denote the structural configuration as $[(\mathrm{AB})_m(\mathrm{C})]_n(\mathrm{AB})_m$. Layers A, B, and C have different refractive indices. Layers $(\mathrm{AB})_m$ can be regarded as Bloch mirrors for the FW and C as nonlinear material defect layer. This is the so-called photonic quantum wells (PQWs). It is noted that the polarization direction of ferroelectric domain of layer C may be inverse. We choose $m = 4$ and $n = 80$ in calculations and assume that layer A (B) is made by the un-poled $\mathrm{BaTiO_3}$ (air) material for determinacy. The refractive index and thickness of layer A (B) are $n_{\mathrm{A}} = 2.4$ ($n_{\mathrm{B}} = 1$) and $d_{\mathrm{A}} = 0.360$ μm ($d_{\mathrm{B}} = 0.640$ μm), respectively. Layer C is chosen as the poled $\mathrm{LiNbO_3}$ crystal with a thickness of $d_{\mathrm{C}} = 3.909$ μm. The intensity of the incident FW wave sets $I = 1.328 \times 10^9 \mathrm{W/m}^2$, corresponding to $|E^{(1)}_{1\omega}(x_1)|^2 = 1.00\ \mathrm{V}^2/\mu\mathrm{m}^2$.

We calculate the transmission probability spectrum, as displayed in Fig. 6: (a) for the perfect truncated (AB) PC , i.e., $d_{\mathrm{C}} = 0.0$ μm; and (b) for the multiple PQWs made of nonlinear material. It is obviously seen from Fig. 6(a) that there exist PBGs in the wavelength ranges of $0.590 - 0.615$ μm, $0.712 - 0.793$ μm, and $0.942 - 1.08$ μm. It is also seen from Fig. 6(b) that there are three strong peaks located within the PBG of 0.942 to 1.080 μm, corresponding to defect modes. One of the defect modes just takes aim at 1.064 μm. To obtain high conversion efficiency, we select the FW wavelength to be 1.064 μm. The arrangement of polarization direction of Layer C should be optimized with the use of the SA algorithm for implementing SHG with the highest conversion efficiency. The objective function used in the SA is chosen as

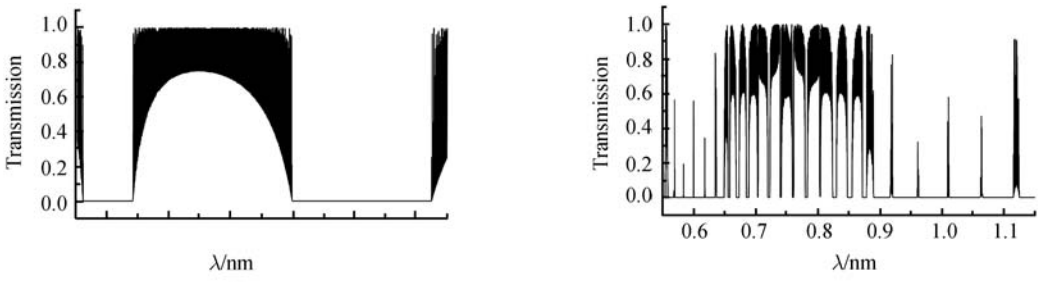

Fig. 6 Transmission spectrum of the FW for two samples : **(a)** One is the perfect truncated (AB) PC; The layer A (B) is made by the un-poled $BaTiO_3$ (air) material; **(b)** the other is composed of alternatingly stacked dielectric-air-nonlinear material layers with finite number and surrounded by air, i.e., $[(AB)_4C]_{80}(AB)_4$. Layers A, B, and C possess different refractive indices. This is the so-called photonic quantum well structures (PQWs).

$$D = |\eta_1^0 - \eta_{\rm forth}(\lambda)| + |\eta_2^0 - \eta_{\rm back}(\lambda)| \tag{3.3.1}$$

where $\lambda = 1.064\ \mu$m and $\eta_{1,2}^0$ is the preset constants. By choosing different values of η_1^0 and η_2^0, the conversion efficiencies of the "forward" and "backward" waves can be tailored.

We first set $\eta_1^0 = 0$ and $\eta_2^0 = 1$, which corresponds to the sample producing dominant 'backward' SHG. The calculated conversion efficiencies are $\eta_{\rm forth} = 3.04 \times 10^{-4}$ and $\eta_{\rm back} = 2.20 \times 10^{-2}$. It is apparent that the $\eta_{\rm back}$ is 72 times that of $\eta_{\rm forth}$. When setting $\eta_1^0 = 1$ and $\eta_2^0 = 0$, we can construct a sample for implementing dominant "forward" SHG. The calculated conversion efficiencies are $\eta_{\rm forth} = 4.18 \times 10^{-2}$ and $\eta_{\rm back} = 1.11 \times 10^{-3}$. We can also design an optimal structure for performing nearly identical conversion efficiency of both the 'forward' and 'backward' SHGs, for instance, by changing the values of η_1^0 and η_2^0, we can construct the sample with $\eta_{\rm forth} = 2.56 \times 10^{-2}$ and $\eta_{\rm back} = 2.58 \times 10^{-2}$. Note that in this sample, the conversion efficiency is significantly enhanced two orders of magnitude, compared to the prefect optical superlattice, which is made of the poled $LiNbO_3$ crystal of 80-layers of alternatingly inverting polarization direction of domain and each layer thickness is $3.428\ \mu$m for matching the QPM condition.

Now, we propose an effective method to design a sample to have the specified defect modes. The SHG conversion efficiency can be significantly enhanced in this sample when the wavelength of FW aims at that of the defect mode. We consider a model structure of alternatingly stacked layers of nonlinear material and air, sandwiched by two truncated PCs. First, we discuss a prototype PC comprised of 10-period alternately stacked A($BaTiO_3$)−B (air) layers, surrounded by air. This PC will be used in the following PQWs structure, which is inserted into the prototype PC. For the convenient description, we denote this prototype PC with a finite number of layers as $(AB)_{10}$. The thicknesses of the constituent layers are $d_{\rm A} = 0.12\ \mu$m and $d_{\rm B} = 0.28\ \mu$m; their refractive indices are $n_{\rm A} = 2.4$ for un-poled $BaTiO_3$ and $n_{\rm B} = 1.0$ for air. We calculate the transmission spectrum of the truncated PC structure with the use of the transfer-matrix method, and there exists a well-defined band gap ranging from $\lambda_a = 0.9069$ to $\lambda_b = 1.5208\ \mu$m.

We then turn to discuss the PQW structure, which is composed of alternatingly stacked-layers of the other two constituents with the refractive indices of $n_{\rm C}$ (for single-orientation poled $LiNbO_3$) and $n_{\rm D}$ (for air), sandwiched by two truncated PCs on either side. The thickness of unit layer is chosen as $d_{\rm C} = d_{\rm D} = 0.02\ \mu$m. However, the real thicknesses of layers C or D may be different from $d_{\rm C} = d_{\rm D}$. They are determined by the requirement of the specified defect states to assign to the pre-assigned wavelengths with the use of the SA algorithm. The whole sample consists of $(AB)_5[CD]_{100}(AB)_5$, and the total length of sample is 6 μm. To design the defective PC with three defect states located at the preset wavelengths of $\lambda_1^0 = 0.9720$, $\lambda_2^0 = 1.0820$, and $\lambda_3^0 = 1.283\ \mu$m. We employ the SA algorithm and define an object function as

$$\begin{aligned} D = &\sum_{\alpha}\sum_{s}\left[|\lambda_\alpha^o - \lambda_\alpha^{(s)}| + \gamma_1|t^0 - t_\alpha^{(s)}|\right] \\ &+\gamma_2\left[\max\{t_\alpha^{(s)}\} - \min\{t_\alpha^{(s)}\}\right] \\ &\lambda_\alpha^o, \lambda_\alpha^{(s)} \in [\lambda_{\alpha-1},\ \lambda_\alpha], \quad \alpha = 1,2,3 \end{aligned} \tag{3.3.2}$$

with

$$\lambda_0(=\lambda_a) < \lambda_1^o < \lambda_1 < \lambda_2^0 < \lambda_2 < \lambda_3^0 < \lambda_3(=\lambda_b)$$

where γ_1 and γ_2 are two adjustable constants, $\lambda_\alpha^{(s)}$ and $t_\alpha^{(s)}$ $(\alpha = 1,2,3)$ denote the wavelength of the defect mode and transmittance, generated from every temporal configuration of the PQWs during the SA process. The optimal design of the PQWs corresponds to a search for the minimum of D through adjusting the refractive index of the individual unit

layer, and selecting one of $n_{\rm C}$ and $n_{\rm D}$; finally, the favorable arrangement of the PQWs can be completely determined.

We carry out the particular design of PQWs for producing three defect states at 0.9720, 1.0820, and 1.2830 μm within the PBG of $[0.9069, 1.5208]\,\mu$m. The structure of the obtained PQW is fully aperiodic. Its transmission spectrum is displayed in Fig.7. It is found that the band gap basically remains unchanged, ($[0.8968,\ 1.5607]\,\mu$m) compared with that of the perfect PC. There exist four strong transmission peaks, three of them correspond to the desirable defect modes. They are located at $\lambda_1 = 0.9681$ μm with a transmittance of 0.949, $\lambda_2 = 1.0796$ μm with a transmittance of 0.965, $\lambda_3 = 1.2811\,\mu$m with a transmittance of 0.997, and an extra stray mode at $\lambda_4 = 1.4648\,\mu$m with a transmittance of 0.774. The positions of defect states accord well with the preset ones, with only a little deviation.

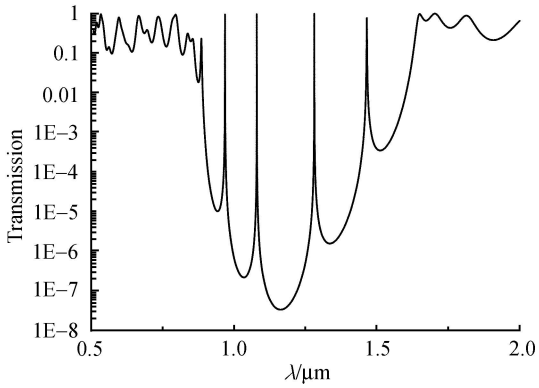

Fig. 7 Transmission spectrum of the FW in the constructed PQW sample for normally incident EM wave with the TE polarization. The PQW structure is composed of alternatingly stacked-layers of other two constituents with the refractive indices of $n_{\rm C}$ (for single-orientation poled $LiNbO_3$) and $n_{\rm D}$ (for air), sandwiched by two truncated PCs on its either sides, i.e., $(AB)_5[CD]_{100}(AB)_5$. The thickness of unit layer is chosen as $d_{\rm C} = d_{\rm D} = 0.02$ μm. However the real thicknesses of layers C or D may be different from $d_{\rm C} = d_{\rm D}$. They are determined by the requirement of the specified defect states to aim at the pre-assigned wavelengths in terms of the SA algorithm.

We turn to reveal the feature of the SHGs of the constructed sample. The intensity of the incident FW wave sets $I = 1.0 \times 10^8 {\rm W/m}^2$. We calculate the SHG conversion efficiency of the constructed sample. It is found that the conversion efficiency $\eta_{\rm back}$ of the backward SHG at the wavelength λ_1 is 0.0188, and $\eta_{\rm forth} = 0.0134$. The conversion efficiency $\eta_{\rm back}$ of the backward SHG at the wavelength λ_2 is 0.0358, and $\eta_{\rm forth} = 0.0365$. Both the conversion efficiencies are almost identical. In contrast, the conversion efficiency $\eta_{\rm back}$ of the backward SHG at the wavelength λ_3 is 0.0156, much larger than $\eta_{\rm forth} = 0.004\,82$. We also consider the counterpart of the above-mentioned sample except for the absence of PQWs; the sample has the same total thickness and under the illumination of the same intensity of the incident FW, its SHG conversion efficiency only reaches $\sim 10^{-12}$. The enhancement of SHG conversion efficiency in the defective photonic crystals is generated from defect mode with much higher density of EM electromagnetic modes and a low group velocity.

4 Summary

The characteristics of the SHGs in two kinds of structures are investigated. The first kind of structure is AOS, in which linear susceptibility is homogeneous, while second-order nonlinear susceptibility is modulated by alternating laminar domains with positive or negative polarization. For the second kind of structure, both linear and nonlinear susceptibilities are inhomogeneous. We derive the general solutions of SHGs for AOSs with finite lateral width and of SHGs in the consideration of the depletion of pump light power of FW. We carry out the design of AOSs in terms of SA algorithm and show that the constructed AOSs can implement multiple wavelength SHG with identical effective nonlinear coefficient at the preassigned wavelengths of incident light. We demonstrate the variations of the effective nonlinear coefficient with the optical wave propagating distance from the surface of the sample and they exhibit monotonously increasing behavior. This clearly infers that the contribution of every block to the optical SHG process is constructive accumulation. We observe giant enhancement of SHGs in the 1D PCs with defects consisting of multiple PQWs made of ferroelectric nonlinear material when the FW frequency takes aim at one of the defect states. We indicate that both forward and backward SHGs can be controlled by adjusting polarization directions of ferroelectric domains. We propose an effective design approach of the structures, which are constructed by aperiodically stacked layers of nonlinear material and air, sandwiched by two truncated PCs, in terms of the SA algorithm. The constructed structure can realize multiple-wavelength SHGs at the preassigned wavelengths. Numerical simulations show that the conversion efficiency of SHG can be significantly enhanced when the FW frequencies aim at the defect states. The origin of the enhancement can be attributed to the high intensity of EM fields of the defect modes and efficient coupling of waves. It is believed that the proposed design approach may provide an instructive and useful way to diversify nonlinear optical materials for matching with various practical applications.

Acknowledgements This work was supported by the Chinese Na-

tional Key Basic Research Special Fund (973 Plan) under Grant No. 2006CB302901, and Chinese Young Science Fund under Grant No. 10604042.

References

1. Yariv A. and Yeh P., Optical Wave in Crystal, New York: Wiley, 1984: 504
2. Shen Y. R., The Principles of Nonlinear Optics, New York: Wiley, 1984
3. Armstrong A, Bloembergen N., Ducuing J., and Pershan P. S., Phys. Rev., 1962, 127: 1918
4. Zhu S. N., Zhu Y. Y., and Ming N. B., Science, 1997, 278: 843
5. Zhu S. N., Zhu Y. Y., Qin Y. Q., Wang H. F., Ge C. Z., and Ming N. B., Phys. Rev. Lett., 1997, 78: 2752
6. Zhu S. N., Zhu Y. Y., Zhang Z. Y., Shu H., Wang H. F., Hong J. F., Ge C. Z., and Ming N. B., J. Appl. Phys., 1995, 77: 5481
7. Meyn J. P. and Fejer M. M., Opt. Lett., 1997, 22: 1214
8. Miller G. D., Batchko R. G., Tulloch W. M., Weise D. R., Fejer M. M., and Ber R. L., Opt. Lett., 1997, 22: 1834
9. Feng D., Ming N. B., Hong J. H., Yang Y. S., Zhu J. S., Yang Z., and Wang Y. N., Appl. Phys. Lett., 1980, 37: 607
10. Xue Y. H., Ming N. B., Zhu J. S., and Feng D., Acta Phys. Sin., 1983, 32: 1515
11. Xue Y. H., Ming N. B., Zhu J. S., and Feng D., Chin. Phys. 1984, 4: 554
12. Thompson D. E., McMullen J. D., and Anderson D. B., Appl. Phys. Lett., 1973, 29: 113
13. Deway C. F. and Hocker L. O., Appl. Phys. Lett., 1975, 26: 442
14. Gu B. Y., Dong B. Z., Zhang Y. and Yang G. Z., Appl. Phys. Lett., 1999, 75: 2175
15. Gu B. Y., Zhang Y. and Dong B. Z., J. Appl. Phys., 2000, 87: 7629
16. Lee Y. W., Fan F. C., Huang Y. C., Gu B. Y., Dong B. Z., and Chou M. H., Opt. Lett., 2002, 27: 2191
17. Dumeige Y., Vidakovic P., Sauvage S., Sagenes I., Levenson J. A., Sibilia C., Centini M., Aguanno G. D., and Scalora M., Appl. Phys. Lett., 2001, 78: 3021
18. Scalora M., Bloemer M. J., Manka A. S., Dowling J. P., Bowden C. M., Viswanathan R., and Haus J. W., Phys. Rev. A. 1997, 56: 3166
19. Centini M., Sibilia C., Scalora M., DAguanno G., Bertolotti M., Bloemer M. J., Bowden C. M., and Nefedov I., Phys. Rev. E, 1999, 60: 4891
20. Ren F. F., Li R., Cheng C., Wang H. T., Qiu J., Si J., and Hirao K., Phys. Rev. B, 2004, 70: 245109
21. Li Z. Y., Gu B. Y., and Yang G. Z., Phys. Rev. B, 1998, 60: 10644
22. Zhao L. M., Gu B. Y., Zhou Y. S., and Wang F. H., J. Phys.: Condens. Matter, 2003, 15: 4889
23. Kirkpatrick S., Gelatt C. D., and Vecchi M. P., Science, 1983, 220: 671
24. Kirkpatrick S ., J. Stat., Phys., 1983, 34: 975
25. Zhao L. M., Gu B. Y., Yang G. Z., and Zhou Y. S., J. Non. Opt. Phys. Mater., 2005, 14: 115
26. Zhao L. M. and Gu B. Y., Appl. Phys. Lett., 2006, 88: 122904
27. Zhao L. M. and Gu B. Y., Opt. Lett., 2006, 31: 1510
28. Dmitriev V. G., Gurazdyan G. G., and Nikogosyan D. N., Handbook of Nonlinear Optical Crystals, Berlin: springer, 1997, Chapt. 3